Ultrafast Photodynamics of Cyano-Functionalized [FeFe]-Hydrogenase Model Compounds

Christopher J. Stromberg, Department of Chemistry and Physics, Hood College, 401 Rosemont Avenue, Frederick, Maryland 21701-8524, United States

Edwin J. Heilweil,* Engineering Physics Division, Physical Measurement Laboratory, National Institute of Standards and Technology, Gaithersburg, MD 20899-8443 United States

Abstract

[FeFe]-hydrogenases are efficient enzymes that produce hydrogen gas under mild conditions. Synthetic model compounds containing all CO or mixed CO/PMe_3 ligands were previously studied by us and others with ultrafast ultraviolet (UV) or visible pump-infrared (IR) probe spectroscopy (TRIR) in an effort to better understand the function and interactions of the active site with light. Studies of anionic species containing cyano groups, which more closely match the biological active site, have been elusive. In this work, two model compounds dissolved in room temperature acetonitrile solution were examined: $[Fe_2(\mu\text{-}S_2C_3H_6)(CO)_4(CN)_2]^{2-}$ (**1**) and $[Fe_2(\mu\text{-}S_2C_2H_4)(CO)_4(CN)_2]^{2-}$ (**2**). These species exhibit long-lived transient signals consistent with loss of one CO ligand with potential isomerization of newly formed ground electronic state photoproducts, as previously observed with all-CO and CO/PMe_3 containing models. We find no evidence for fast (ca. 150 ps) relaxation seen in the all-CO and CO/PMe_3 compounds because of the absence of the metal-to-metal charge transfer band in the cyano-functionalized models. These results indicate that incorporation of cyano ligands may significantly alter the electronic

properties and photoproducts produced immediately after photoexcitation, which may influence the catalytic activity of model compounds when attached to photosensitizers.

*Corresponding author: Edwin.heilweil@nist.gov

Introduction

The [FeFe]-hydrogenases are exceptionally efficient enzymes that reduce protons to hydrogen gas under mild conditions.[1-11] The active site of the enzyme contains a di-iron moiety with two attached bridging sulfur ligands as well as pendant CO and CN ligands. The molecular structure of the native enzyme's active site in one oxidation state is shown in Figure 1.[1, 9, 12-14] It has also been shown that CO can passivate the enzyme and the oxidized form of the enzyme can be regenerated by exposure to white light. [2, 15] Many model compounds have been synthesized as a means to understand the functionality of the [FeFe]-hydrogenases, and these models are also potential catalysts in their own right.[16-26]

Some of the model systems have been designed to include a photosensitizer to activate the reduction reaction by absorption of light.[27-37] However, the photo-dynamics of the di-iron active site alone when exposed to light are not well understood. Model compounds containing all CO or mixed CO and PMe_3 ligands have been examined using ultrafast ultraviolet (UV) or visible (Vis) excitation, infrared (IR) probe spectroscopies (TRIR and 2DIR, including our TRIR work[37,39]) to better understand the interactions of the active site with light.[38-46] Models containing cyano ligands, which more closely match the biological active site, have been synthesized and studied using other methods for years,[18, 22-23, 25, 47-57] but they have been more difficult to study using TRIR methods due solubility issues and low signals.[58-59]

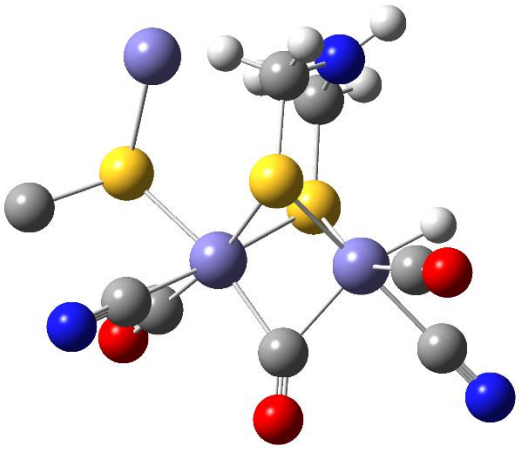

Figure 1. General structure of the [FeFe]-Hydrogenase active site with bridging amino group, three CO and two CN pendant ligands.[1, 9, 12-14]

In this work, the photo-dynamics of two model compounds were examined in room temperature acetonitrile solution: $[Fe_2(\mu\text{-}S_2C_3H_6)(CO)_4(CN)_2]^{2-}$ (**1**) and $[Fe_2(\mu\text{-}S_2C_2H_4)(CO)_4(CN)_2]^{2-}$ (**2**). Each of these compounds potentially exists in multiple isomeric forms (five for **1** and four for **2**) at room temperature. As examples, the dominant isomers found in each crystal structure are shown in Figure 2.[18] We find that these two model systems exhibit long-lived transient TRIR signals consistent with rapid (20-30 ps) vibrational cooling followed by loss of a CO ligand and possible isomerization of ground electronic state photoproducts, as was previously observed with all-CO and CO/PMe_3 species.[38, 40-42, 46, 60] However, the resultant data for the cyano-containing compounds does not show evidence for the fast (ca. 150 ps) decay observed in previous studies of the all-CO and mixed CO/PMe_3 model compounds. This new observation is apparently due to the absence or decreased intensity of the metal-to-metal charge transfer band in the cyano-functionalized models. These results indicate that incorporation of

cyano ligands can significantly alter the photoproducts produced immediately after excitation, which may influence the catalytic activity of designed photosensitized derivatives.

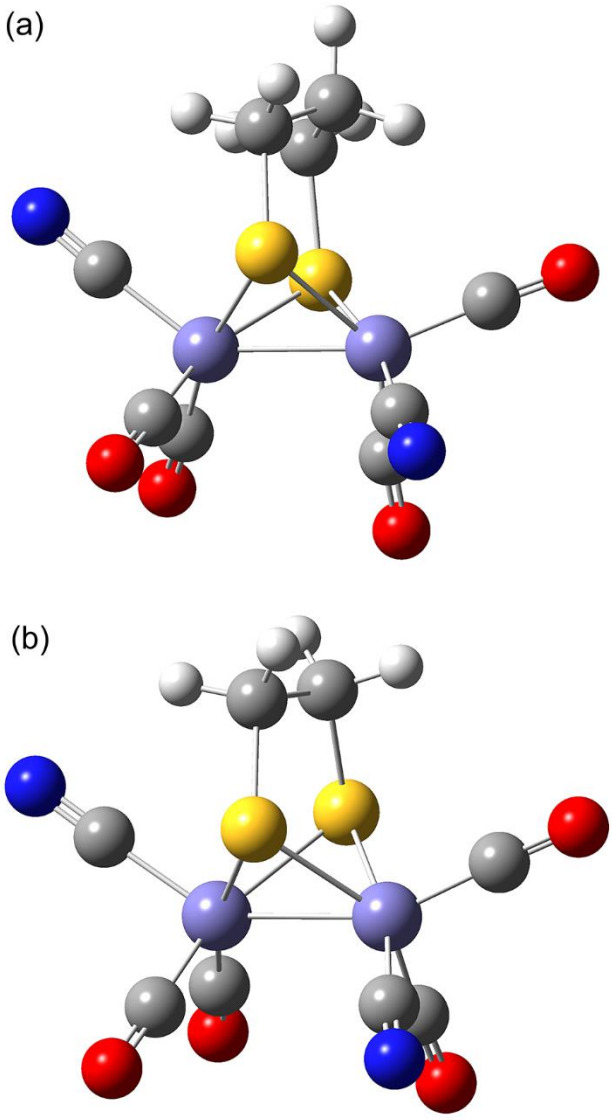

Figure 2. Dominant crystal equatorial-axial crystal isomer structures of (a) $[Fe_2(\mu\text{-}S_2C_3H_6)(CO)_4(CN)_2]^{2-}$ (**1**) and (b) $[Fe_2(\mu\text{-}S_2C_2H_4)(CO)_4(CN)_2]^{2-}$ (**2**).[18]

Experimental Methods

Synthesis

Syntheses of **1** and **2** were conducted according to literature methods[18] and summarized as follows: $Fe_2(\mu\text{-}S_2C_3H_6)(CO)_6$ (**3**) and $Fe_2(\mu\text{-}S_2C_2H_4)(CO)_6$ (**4**) were synthesized by combining triiron-dodecacarbonyl with 1,3-propane dithiol or 1,2-ethane dithiol, respectively. **1** (**2)** was synthesized by combining **3** (**4)** with two equivalents of $[N(C_2H_5)_4]CN$, resulting in $[N(C_2H_5)_4]_2[Fe_2(\mu\text{-}S_2C_3H_6)(CO)_4(CN)_2]$ **1** ($[N(C_2H_5)_4]_2[Fe_2(\mu\text{-}S_2C_2H_4)(CO)_4(CN)_2]$ **2)** in acetonitrile. Solids were collected after solution precipitation and recrystallized for purification and examined as ca. 1 mM concentration solutions under argon in room temperature (293 K) acetonitrile. Infrared spectra of the resultant solutions agreed with those previously published.[17]

Time-Resolved UV Pump/IR Probe Laser Spectroscopy

The output of a 30 fs, 80 MHz Ti:Sapphire oscillator (Kapteyn-Murnane Lasers)[61] tuned to 800 nm was used to seed a home-built Ti:Sapphire linear cavity, single Pockels cell regenerative amplifier. The resulting 800 nm, 80 fs, 700 μJ pulses produced at 1 kHz repetition rate were used to pump a Spectra-Physics OPA-800F optical parametric amplifier (OPA). The OPA signal and idler output beams were difference frequency mixed using a AgGaS crystal yielding 120 fs, ca. 1 μJ mid-IR pulses with a 230 cm^{-1} full-width at half maximum (FWHM) centered around 2000 cm^{-1} (5 micrometer wavelength, CN- and CO-stretching mode region).

Sample excitation (pump) pulses were generated using residual 800 nm light from the OPA as either doubled (400 nm, 70 fs) or tripled (266 nm, 60 fs) sources. These wavelengths overlap reasonably closely to absorptions observed in the UV-Vis spectra for both molecules, as

shown in Figure 3. Pumping with different wavelengths is important, as some [FeFe]-hydrogenase model compounds show strong differences when excited at different frequencies.[38]

The pump beam (UV or visible) was overlapped with the IR probe beam and transmitted through the sample. Samples were contained in a 2 mm pathlength double CaF_2 windowed flow cell which is also mechanically raster scanned during spectral and time-delayed data acquisition to reduce the possibility of product build-up on the front window. A separate IR beam derived upstream by a 50 % beamsplitter was also directed through the sample away from the pump pulse to serve as a spectral reference on each laser shot. Relative pump-probe pulse timing was produced by a computer-controlled 50 mm optical delay stage (300 ps maximum delay) along the IR beam path. The IR and reference beams were sent through a scanning monochromator (4 cm^{-1} resolution) onto matched single-element amplified mercury-cadmium-telluride detectors with pulsed output voltages sampled on each laser shot via two boxcar averagers (Stanford Research Systems model 250)[61] and their outputs digitized for computer controlled data acquisition and post-processing. Transient spectra displayed below were typically obtained by averaging 1000 laser shots per spectral point (at 2 cm^{-1} steps) and two independent runs further averaged to obtain highest signal-to-noise with ca. 0.001 OD noise (type b, k=2 averages). Kinetic scans were obtained by averaging 1000 laser shots per delay position with further averaging several decay datasets. All measurements were conducted at 293K.

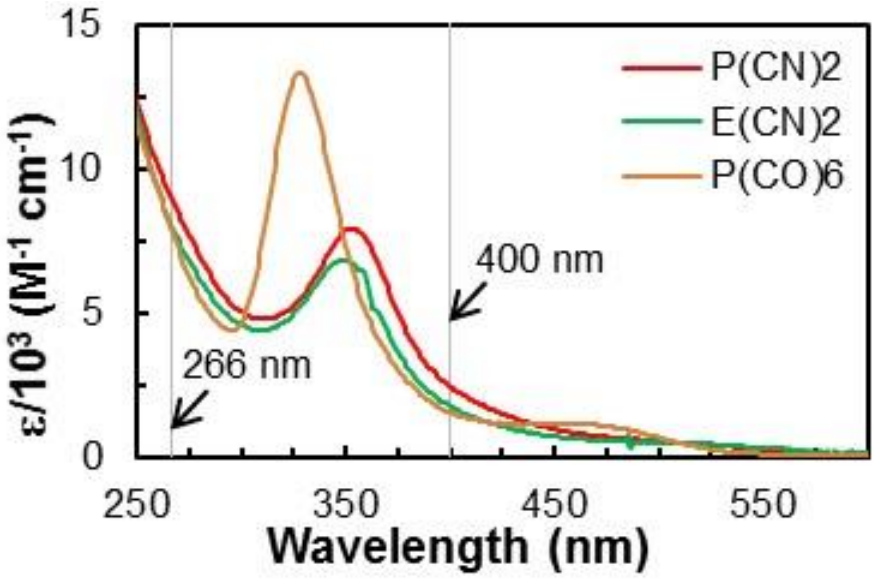

Figure 3. Ultraviolet-visible extinction spectra of model Fe-Fe hydrogenase species **1** (red), **2** (green) and for comparison the hexacarbonyl ligated compound **3** (brown) dissolved in room temperature acetonitrile solution**.**

Calculations

Predicted CO-stretch and CN-stretching mode wavenumber and absorption intensities were calculated with Density Functional Theory (DFT)[62] using the Gaussian 09W[63] software package. These gas phase, lowest energy structure model calculations employed the BP86 functional[64-66] with a TZVP basis set.[67-68] Bandwidths appropriate for metal-carbonyls dissolved in acetonitrile (9 cm^{-1} FWHM) were convoluted with the resultant spectra to simulate experimental infrared solution absorption spectra of ground state and isomeric structures of these model compounds

Results and Discussion

Steady-State mid-IR Spectra

As mentioned previously, compound **1** may be present as five isomeric structures but for **2** only four possible isomers may exist (isomers 2 and 3 only differ by the position of the middle, bridging carbon, which does not exist in the ethyl-bridged **2**). These possible isomeric structures are shown in Figure 4. Each isomer is predicted to have a unique spectrum in the infrared, as shown for **1** in Figure 5. The best match to the experimental spectrum (see Figure 5 (a)) is found assuming that only the most polar isomer **1-5** will be present in polar acetonitrile solution. A similar analysis predicts that isomer **2-5** is the most likely stable form of **2** in the investigated TRIR sample (see Figure S1) and equivalent experimental and calculated ground state infrared spectra for **2** are shown in Figure S2. Solvent-dependent shifts between isomers have been observed for other [FeFe]-hydrogenase model compounds,[40-41, 69] but previous work identified only a single isomer for **1** in acetonitrile.[18] The energy differences for isolated gas-phase molecules, as calculated using DFT, are shown in Figure 4 (these energy differences are similar to those seen in the model compounds with two trimethylphosphine ligands, rather than two cyano ligands).[40, 69] Assignments for the CO and CN vibrational stretches can be found in the supplementary information Table S1)

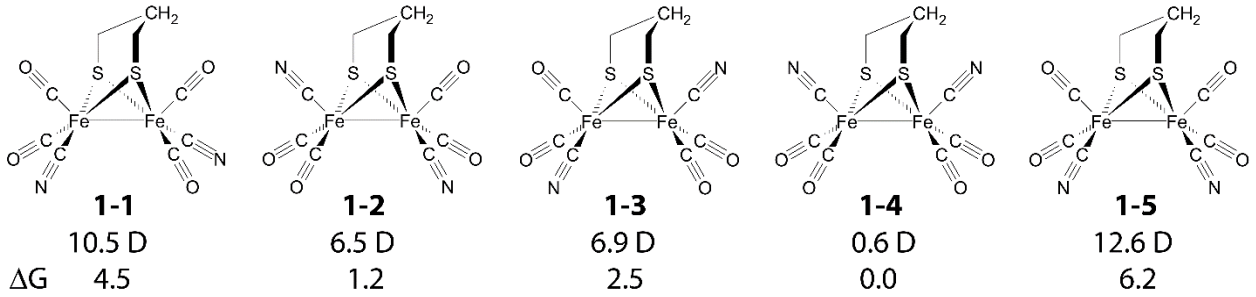

Figure 4. Possible isomers of model compound **1**. Dipole moments (Debyes) and energy difference (kcal/mol) are shown for the gas-phase, isolated molecules, as calculated by DFT. Isomer **1-2** is reported in the x-ray crystal structure[18] while **1-5** is the most likely dominant isomer in acetonitrile solution based on the calculated spectra and polarities shown.

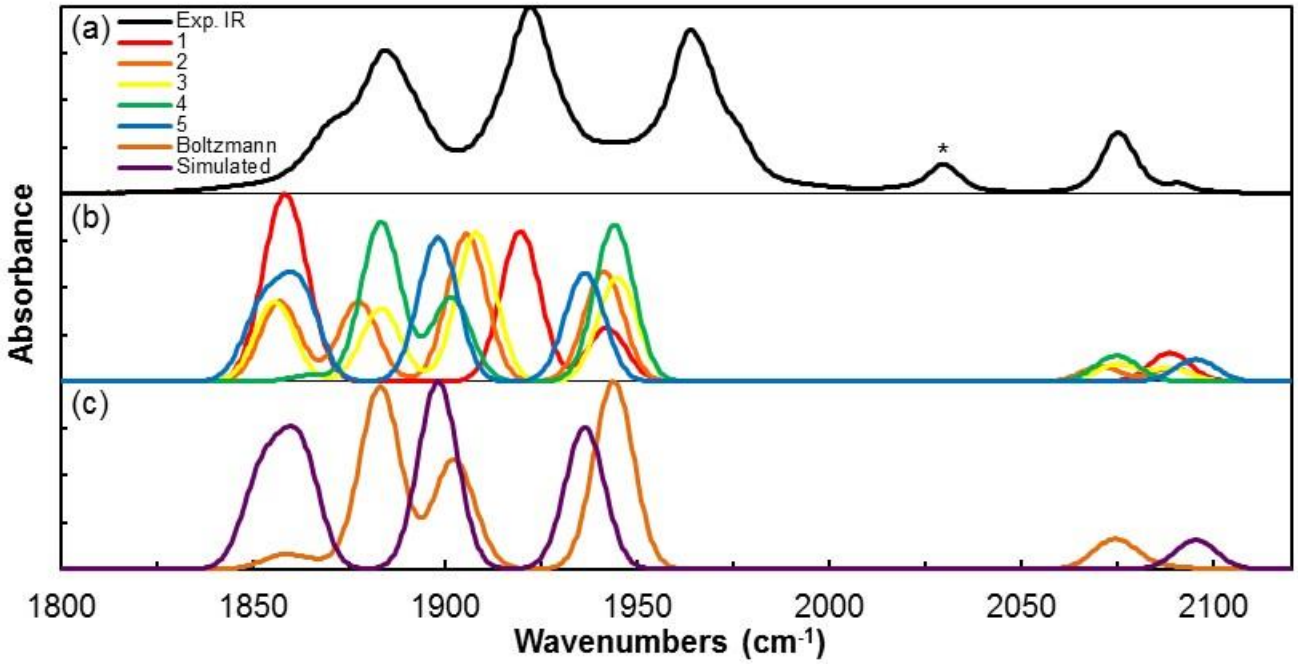

Figure 5. (a) Experimental infrared spectrum of **1** in acetonitrile. The band marked with an asterisk is from a small amount of $[Fe_2(\mu\text{-}S_2C_3H_6)(CO)_5(CN)_1]^-$ present in the sample. (b) Simulated IR spectra of each isomer of **1** based on DFT calculations with (c) comparison of simulated IR spectra assuming a Boltzmann distribution of isomers (brown) and only isomer **1- 5** (purple).

Time-Resolved TRIR Spectroscopy

Figure 6 shows the measured TRIR spectra of **1** in acetonitrile at a number of pump-probe delay times when employing 266 nm (Figure 6(a)) and 400 nm (Figure 6(b)) pump wavelength. Figure 7 depicts detailed time-resolved dynamics obtained with the monochromator set to particular probe spectral wavelengths of interest. In the time-delayed data, three timescales are readily extracted from averaged global fitting: a very fast 0.28 ± 0.058 ps decay (see the lowest wavenumber absorptions and bleaches) followed by a 20 ± 10 ps decay and a long-lived offset. Very similar timescales are observed for **2**: a fast 0.35 ± 0.10 ps decay of new absorption features followed by a 35 ± 15 ps transient and a long-lived offset (data shown in Figures 8 and 9). The <1 ps pulsewidth-limited transient absorption decays most likely arise from a coherence artifact when the pump and probe pulses overlap in the sample. Short ca. 20 ps to 30 ps decays are generally smaller in amplitude for the 266 nm scans. This 20-30 ps decay component has been identified with solute-to-solvent vibrational cooling, perhaps originating from relaxation of the excited state resulting from excitation of the MLCT band.[41, 46, 60] The longest timescale component for both species suggests new (with ns or longer lifetime) photoproducts are generated by both excitation wavelengths.

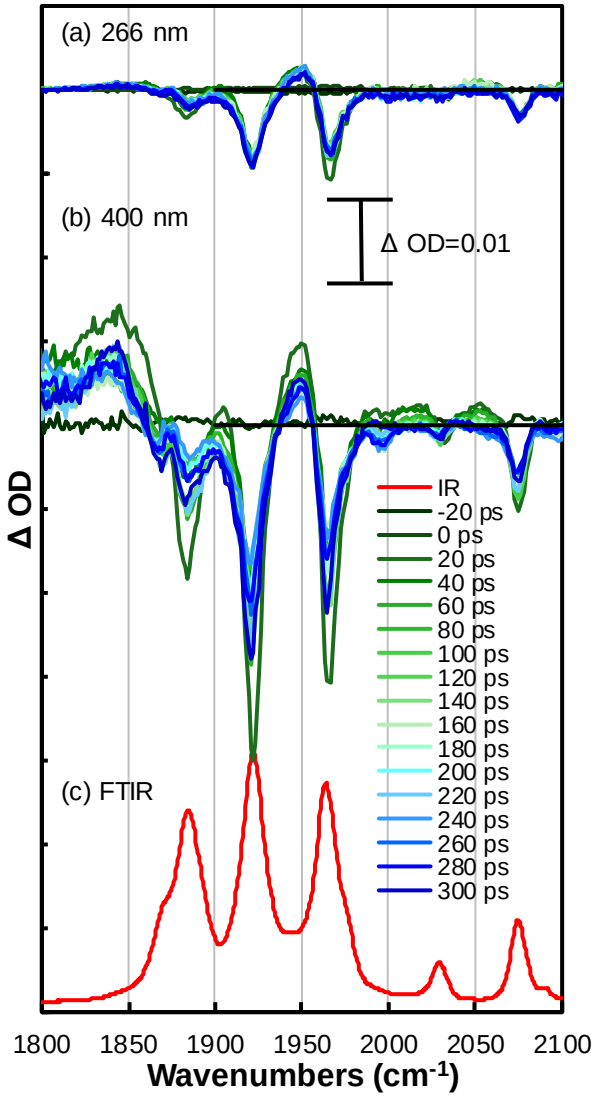

Figure 6. Representative time-resolved UV and visible pump, IR probe spectra for **1** in room temperature acetonitrile at indicated time delays after excitation with (a) 266 nm, (b) 400 nm and (c) ground state FT-IR spectrum of **1** in acetonitrile solution.

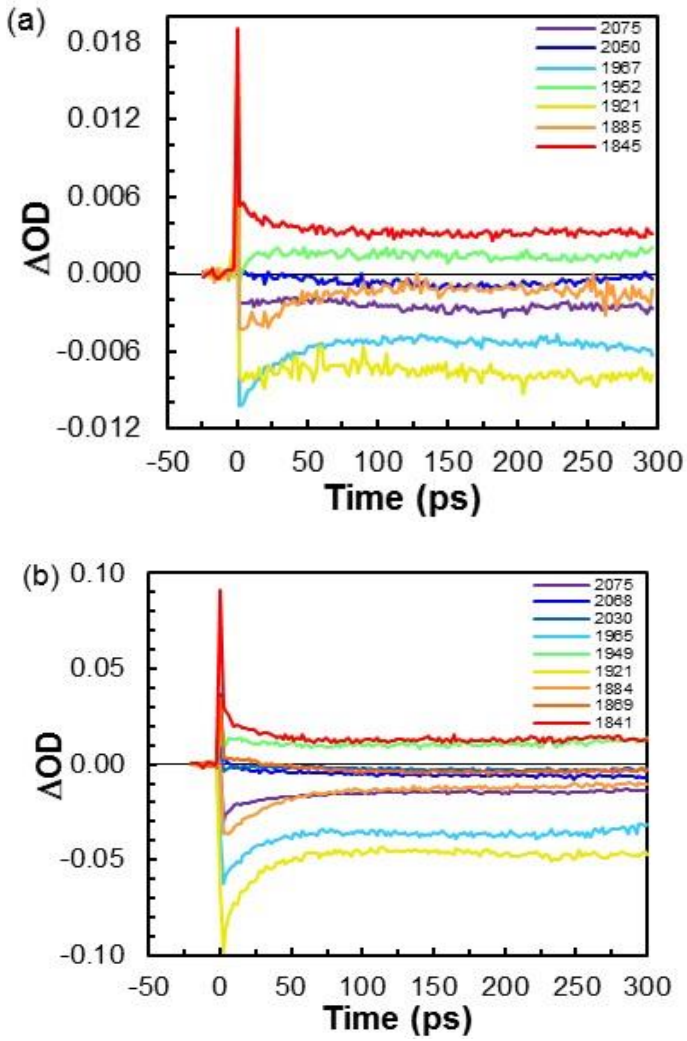

Figure 7. Time-dependent transient decay kinetics of **1** in acetonitrile at indicated IR wavelengths (cm^{-1}) as shown in Figure 6 when using (a) 266 nm and (b) 400 nm pump excitation wavelengths.

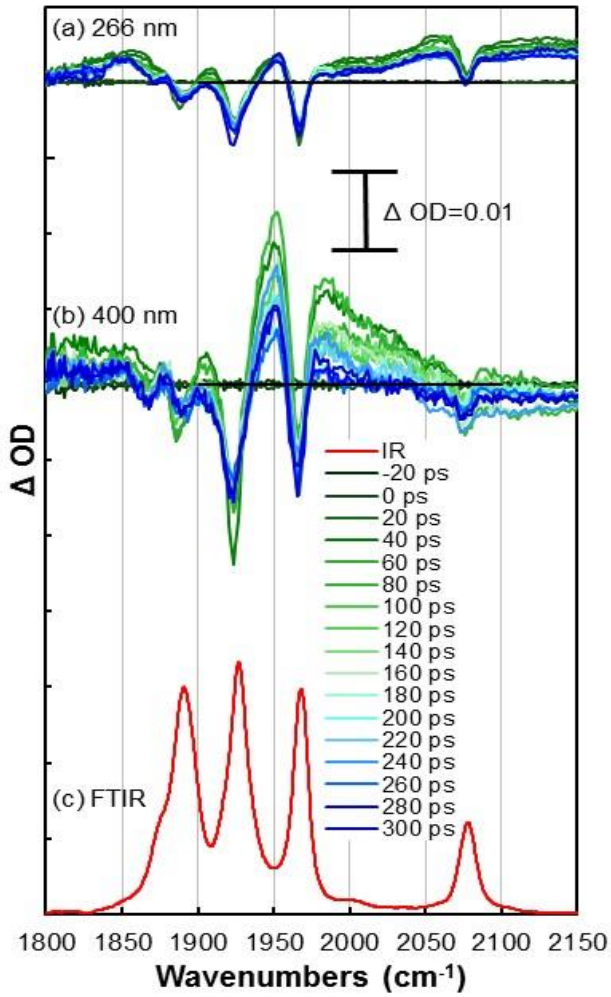

Figure 8. Time-resolved TRIR UV and visible pump, IR probe spectra for **2** in acetonitrile with (a) 266 nm and (b) 400 nm excitation. (c) FT-IR spectrum of **2** in room temperature acetonitrile solution.

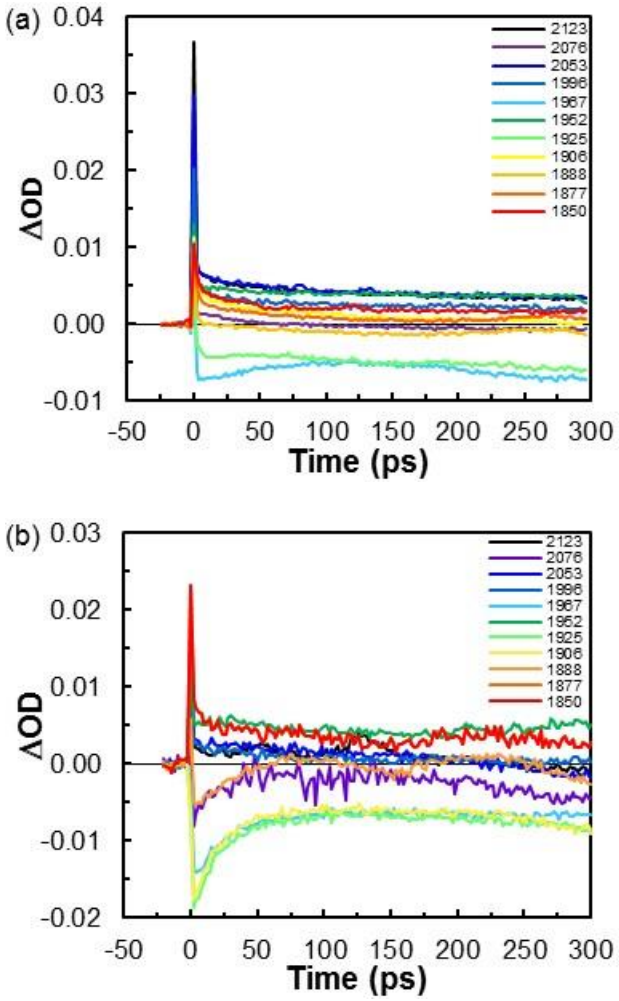

Figure 9. Time-dependent transient decay kinetics of **2** in acetonitrile at selected IR wavelengths (cm^{-1}) as shown in Figure 8 when using (a) 266 nm and (b) 400 nm pump excitation wavelengths.

The long-lived spectra for **1** (dark blue spectra in Figure 6) exhibits two new absorptions at 1840 cm^{-1} and 1951 cm^{-1}. One possible explanation for these long-lived signals is that the compound isomerizes upon either excitation or relaxation to the ground state. This behavior has been reported previously for the di-substituted trimethylphosphine derivative, $Fe_2(\mu\text{-}S_2C_3H_6)(CO)_4(PMe_3)_2$ (**5**).[40-41] However, when comparing the calculated spectra of the

individual isomers shown in Figure 5 to the experimental one, none of the other tetracarbonyl, dicyano isomers exhibit an absorption band lower in energy than the lowest energy band of isomer 5 (at 1870 cm^{-1} in the experimental data but computed to be at 1850 cm^{-1} in the DFT calculations). This behavior suggests that the new strong absorption at 1840 cm^{-1} cannot be explained solely by isomerization but that a new product may be formed.

To explain the origin of the long-lived spectral signatures, DFT calculations were performed to generate the possible CO or CN-loss photoproduct spectra from each isomer (all possible CO- and CN-loss isomers are shown in Figure S3). Full energetics, dipole moments and band frequency results for all fragments are shown in the supplementary information, Tables S2-S7. Example spectral results for some of these calculations are shown in Figure 10 (a) (potential CN-loss photoproducts) and Figures 10 (b) and (c) (potential CO-loss photoproducts). Loss of one CN^- ligand results in a single negative charge on the di-iron core rather than the doubly negative charge on the parent molecule. This results in all CO and CN bands shifting to higher wavenumbers. If a CN were ejected upon UV or visible excitation, there should be no new absorption bands near 1840 cm^{-1} and additional new absorptions would be expected in the 1980 cm^{-1} to 2070 cm^{-1} region, but these are not observed. Thus, when considering the experimental and calculated spectra, there is no evidence for any CN-loss photoproducts.

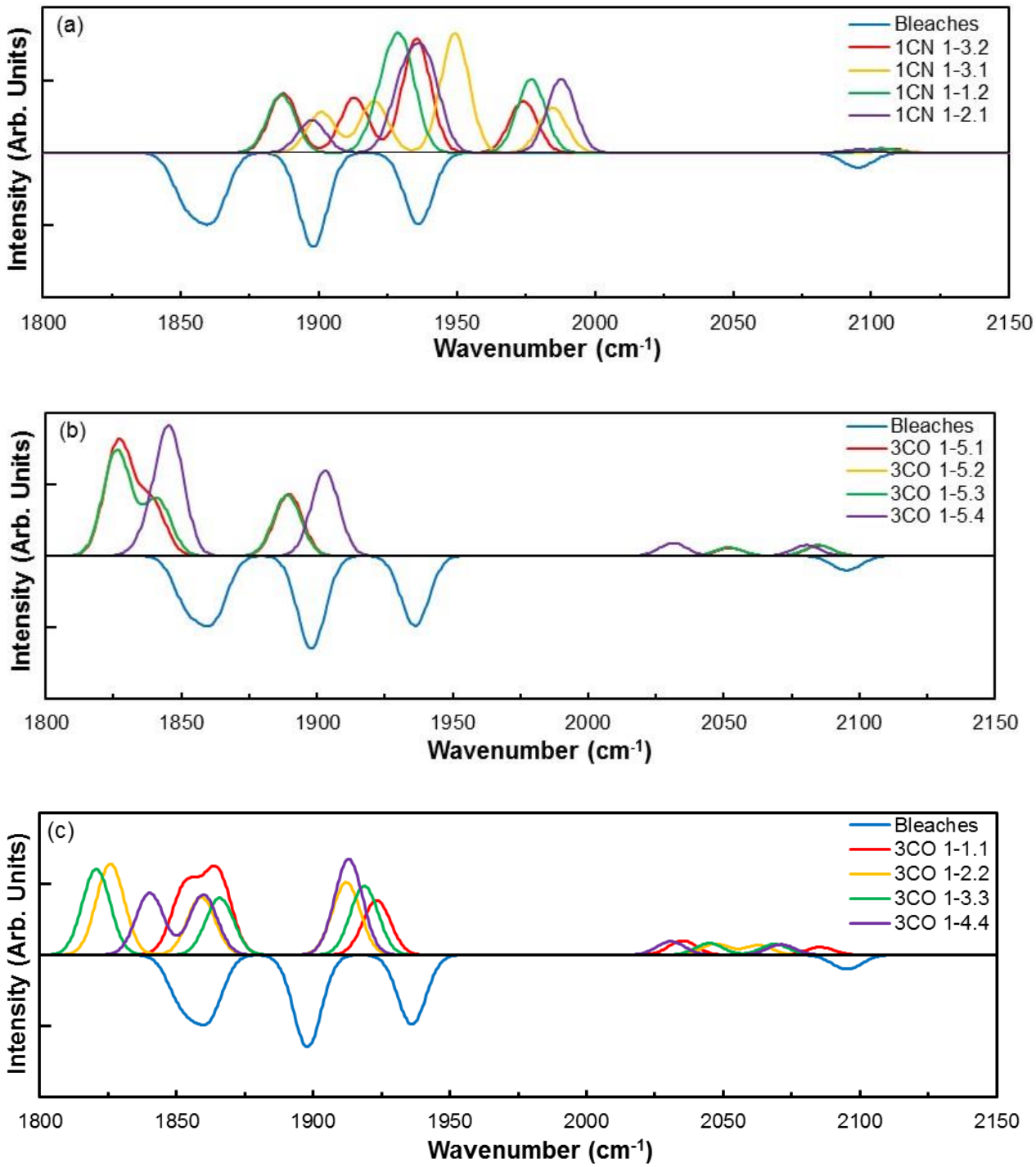

Figure 10. Calculated difference spectra for **1** based on DFT calculations of indicated photoproduct isomers for (a) CN-loss products, (b) CO-loss products from parent isomer **1-5** and (c) CO-loss products from other isomeric forms.

There are four possible CO-loss products derived from isomer **1-5**, with calculated spectra shown in Figure 10 (b) (fragments 1-5-2 and 1-5-3 have essentially identical spectra). Each of these potential photoproducts could explain the appearance of the new absorption band at 1840 cm^{-1}, but none of them are likely to produce a new strong absorption band in the 1950 cm^{-1} range. CO-loss products from other isomers (examples shown in Figure 10 (c)) exhibit bands at both 1840 cm^{-1} and 1950 cm^{-1}. Since isomer **1-5** seems to be the only isomer present in acetonitrile, this would require a geometric rearrangement on a fast timescale along with the CO loss.

A single photoproduct is unlikely, and there are far too many possible photoproducts to narrow down the possibilities much more than this. In the end, the best that can be said is that the photoproducts are probably a complex mixture of tricarbonyl, dicyano products, with some of the photoproducts isomerizing from the starting 1-5 isomer. Some isomerization of tetracarbonyl, dicyano products cannot be ruled out, as well. A similar analysis was found for **2** as the starting species (see Figures S4 and S5).

This analysis is supported by examining the CN-stretching region of the spectra. The band at 2076 cm^{-1} in the FT-IR spectrum of **1** (Figure 6d) results from uncoupled, nearly degenerate vibrations of the two CN ligands. This band becomes a bleach in the TRIR data. At short delay times, a few weak, positive-going features may be seen below this bleach, but at longer delay times, very little, if any, signal occurs in this area. As can be seen in Figure 10b and 10c, CO loss would result in the loss of degeneracy between the two CN vibrations, with the CN on the iron that lost the CO shifting down farther than the CN on the iron with two CO ligands. This results in the intensity from the already weak CN bands being split into two. If a single isomer were formed these signals, although weak, would probably be identifiable. However, if

multiple isomers are formed, one would expect the intensity would be further reduced and frequency-shifted, resulting in very weak signals that would be very difficult to detect. As can be seen in Figure 6, the background subtraction is not perfect, resulting in a baseline that is slightly below zero in the region above the highest CO band (2000 cm^{-1} and above). However, just below the CN bleach, the signal goes up to essentially zero. This might be evidence of a broad set of CN bands resulting from multiple isomers, although, with the imperfect background subtraction, this is difficult to say with any certainty.

The situation in Figure 8 is similar, although the interpretation is complicated by imperfect background subtraction and the sloping baseline in the CN-stretch region. There may be a small, broad, positive-going signal just below the CN stretch, but this is difficult to say for sure. The very weak signals in this area would again be consistent with the intensity being split among a number of CO-loss isomers.

One of the most intriguing and unexpected characteristics of the kinetic data measured for **1** and **2** is the absence of a ca. 150 ps decay observed for all of the other hydrogenase model systems. In every model compound studied to date, a ca. 150 ps decay component was observed and assigned as decay of a long-lived excited electronic state.[38, 40-42, 46] No such decay time is found for either **1** or **2** in this work. This finding may be related to the lack of a weak, broad absorbance band found at around 500 nm for the other model systems (for instance, see the spectrum of **3** shown in Figure 3). This absorption band is present in all other model systems studied so far and was previously assigned to the metal-metal charge transfer transition.[70] Suppression or significantly reduced extinction of this band in the ground state ionic species (perhaps originating from altered charge density on the Fe-Fe core) may explain the lack of observing a 150 ps decay component in **1** and **2**.

Conclusions

The photochemical mechanisms for two cyano-containing model compounds of Fe-Fe Hydrogenase were examined. Compounds **1** and **2** dissolved in room temperature acetonitrile were photo-excited at 266 nm and 400 nm and subsequent photochemistry probed using ultrafast TRIR spectroscopy. Careful comparison of experimental TRIR spectra with calculated DFT results for multiple potentially generated isomeric structures indicates CN^- is not photolytically cleaved, but CO is ejected under both excitation conditions to potentially form multiple ground state isomers. Transient dynamics of newly-formed bleach and absorption features exhibits a <1 ps response (coherent artifact or fast electronic relaxation), ca. 20 ps to 30 ps thermal relaxation decay followed by constant (> ns) spectral bleach and absorption features of newly formed photoproducts. Suppression or significantly reduced extinction of the Fe-Fe metal charge transfer band in the ground state ionic species **1** and **2**, which may originate from altered charge density on the Fe-Fe core, may explain the lack of a longer 150 ps decay component observed for all CO and CO/PMe_3 systems. We propose that from the findings in this work summarized above, it appears that inclusion of CN ligands may directly influence the electronic nature of the wild-type enzyme leading to its high H_2-production turnover rate. Direct comparison to recently investigated related di-iron systems[59, 71] with further DFT modeling of the electronic structures of these product isomers is warranted to try to untangle this possibility.

Acknowledgements

We thank the National Institute of Standards and Technology in Gaithersburg, MD for funding this work via NIST Cooperative Agreement Number 60NANB13D143, Scientific Technical

Research Support (STRS) and use of the TRIR facilities. Additional funding was provided by the Hood College Summer Research Institute.

References

1. Adams, M. W.; Stiefel, E. L. Organomettalic Iron: The Key to Biological Hydrogen Meabolism. *Chem. Biol.* **2000,** *4*, 214-220.
2. Adams, M. W. W.The Structure and Mechanism of Iron-Hydrogenases. *Biochim Biophys Acta.-Bioenergetics* **1990,** *1020*, 115-145.
3. Adams, M. W. W.; Stiefel, E. I. BIOCHEMISTRY: Biological Hydrogen Production: Not So Elementary. *Science* **1998,** *282*, 1842-1843.
4. Bennett, B.; Lemon, B. J.; Peters, J. W. Reversible Cabon Monoxide Binding and Inhibition at the Active Site of the Fe-Only Hydrogenase. *Biochemistry* **2000,** *39*, 7455-7460.
5. Groysman, S.; Holm, R. H. Biomimetic Chemistry of Iron, Nickel, Molybdenum, and Tungsten in Sulfur-Ligated Protein Sites. *Biochemistry* **2009,** *48*, 2310-2320.
6. Hambourger, M.; Gervaldo, M.; Svedruzic, D.; King, P. W.; Gust, D.; Ghirardi, M.; Moore, A. L.; Moore, T. A. [FeFe]-Hydrogenase-Catalyzed H_2 Production in a Photoelectrochemical Biofuel Cell. *J. Am. Chem. Soc.* **2008,** *130*, 2015-2022.
7. Lubner, C. E.; Grimme, R.; Bryant, D. A.; Golbeck, J. H. Wiring Photosystem I for Direct Solar Hydrogen Production. *Biochemistry* **2010,** *49*, 404-414.
8. Nicolet, Y.; Lemon, B. J.; Fontecilla-Camps, J. C.; Peters, J. W., A novel FeS cluster in Fe-only hydrogenases. *Trends Biochem. Sci.* **2000,** *25*, 138-142.
9. Peters, J. W.; Lanzilotta, W. N.; Lemon, B. J.; Seefeldt, L. C. X-ray Crystal Structure of the Fe-Only Hydrogenase (CpI) from Clostridium pasteurianum to 1.8 Angstrom Resolution. *Science* **1998,** *282* (5395), 1853-1858.
10. Shima, S.; Pilak, O.; Vogt, S.; Schick, M.; Stagni, M. S.; Meyer-Klaucke, W.; Warkentin, E.; Thauer, R. K.; Ermler, U. The Crystal Structure of [Fe]-Hydrogenase Reveals the Geometry of the Active Site. *Science* **2008,** *321*, 572-575.
11. Wang, X.-B.; Niu, S.; Yang, X.; Ibrahim, S. K.; Pickett, C. J.; Ichiye, T.; Wang, L.-S. Probing the Intrinsic Electronic Structure of the Cubane [4Fe-4S] CLuster, Nature's Favorite Cluster for Electron Transfer and Storage. *J. Am. Chem. Soc.* **2003,** *125*, 14072-14081.
12. Darensbourg, M. Y.; Lyon, E. J.; Zhao, X.; Georgakaki, I. P. The Organometallic Active Site of [Fe]Hydrogenase: Models and Entatic States. *Proc. Natl. Acad. Sci. U.S.A.* **2003,** *100*, 3683-3688.
13. Nicolet, Y.; Piras, C.; Legrand, P.; Hatchikian, C. E.; Fontecilla-Camps, J. C. Desulfovibrio Desulfuricans Iron Hydrogenase: The Structure Shows Unusual Coordination to an Active Site Fe Binuclear Center. *Structure* **1999,** *7*, 13-23.
14. Popescu, C. V.; Eckard, M. Electronic Structure of the H cluster in [Fe]-Hydrogenases. *J. Am. Chem. Soc.* **1999,** *121*, 7877-7884.
15. Chen, Z.; Lemon, B. J.; Huang, S.; Swartz, D. J.; Peters, J. W.; Bagley, K. A. Infrared Studies of the CO-Inhibited Form of the Fe-Only Hydrogenase from *Clostridium pasteurianum* I: Examination of Its Light Sensitivity at Cryogenic Temperatures. *Biochemistry* **2002,** *41*, 2036-2043.

16. Daraosheh, A. Q.; Harb, M. K.; Windhager, J.; Görls, H.; El-khateeb, M.; Weigand, W. Substitution Reactions at [FeFe] Hydrogenase Models Containing [2Fe3S] Assembly by Phosphine or Phosphite Ligands. *Organometallics* **2009,** *28*, 6275-6280.
17. Gloaguen, F.; Lawrence, J. D.; Rauchfuss, T. B., Biomimetic Hydrogen Evolution Catalyzed by an Iron Carbonyl Thiolate. *J. Am. Chem. Soc.* **2001,** *123*, 9476-9477.
18. Gloaguen, F.; Lawrence, J. D.; Schmidt, M.; Wilson, S. R.; Rauchfuss, T. B. Synthetic and Structural Studies on $[Fe_2(SR)_2(CN)_x(CO)_{6-x}]^{x-}$ as Active Site Models for Fe-Only Hydrogenases. *J. Am. Chem. Soc.* **2001,** *123*, 12518-12527.
19. Harb, M. K.; Apfel, U.-P.; KuÌˆbel, J.; Gorls, H.; Felton, G. A. N.; Sakamoto, T.; Evans, D. H.; Glass, R. S.; Lichtenberger, D. L.; El-khateeb, M.; Weigand, W. Preparation and Characterization of Homologous Diiron Dithiolato, Diselenato, and Ditellurato Complexes: [FeFe]-Hydrogenase Models. *Organometallics* **2009,** *28*, 6666-6675.
20. Harb, M. K.; Niksch, T.; Windhager, J.; Görls, H.; Holze, R.; Lockett, L. T.; Okumura, N.; Evans, D. H.; Glass, R. S.; Lichtenberger, D. L.; El-khateeb, M.; Weigand, W. Synthesis and Characterization of Diiron Diselenolato Complexes Including Iron Hydrogenase Models. *Organometallics* **2009,** *28*, 1039-1048.
21. Lawrence, J. D.; Li, H.; Rauchfuss, T. B. Beyond Fe-only Hydrogenases: N-Functionalized 2-aza-1,3-Dithiolates $Fe_2[(SCH_2)_2NR](CO)_x$ (x = 5,6). *Chem. Commun.* **2001,** , 1482-1483.
22. Le Cloirec, A.; Best, S. P.; Borg, S.; Davies, S. C.; Evans, D. J.; Jughes, D. L.; Pickett, C. J., A Di-Iron Dithiolate Possessing Structural Elements of the Carboyl/Cyande Sub-Site of the H-Centre of Fe-Only Hydrogenase. *Chem. Commun.* **1999**, 2285-2286.
23. Lyon, E. J.; Georgakaki, I. P.; Reibenspies, J. H.; Darensbourg, M. Y. Coordination Sphere Flexibility of Active-Site Models for Fe-Only Hydrogenase: Studies in Intra- and Intermolecular Diatomic Ligand Exchange. *J. Am. Chem. Soc.* **2001,** *123*, 3268-3278.
24. Song, L.-C.; Gao, W.; Feng, C.-P.; Wang, D.-F.; Hu, Q.-M. Investigations on Synthesis, Structure, and Properties of New Butterfly [2Fe2Se] Cluster Complexes Relevant to Active Sites of Some Hydrogenases. *Organometallics* **2009,** *28*, 6121-6130.
25. Tye, J. W.; Darensbourg, M. Y.; Hall, M. B. De Novo Design of Synthetic Di-Iron(I) Complexes as Structural Models of the Reduced Form of Iron-Iron Hydrogenase. *Inorg. Chem.* **2006,** *45*, 1552-1559.
26. Zhao, X.; Georgakaki, I. P.; Miller, M. L.; Yarbrough, J. C.; Darensbourg, M. Y. H/D Exchange Reactions in Dinuclear Iron Thiolates as Activity Assay Models of Fe−H2ase. *J. Am. Chem. Soc.* **2001,** *123*, 9710-9711.
27. Ekström, J.; Abrahamsson, M.; Olson, C.; Bergquist, J.; Kaynak, F. B.; Eriksson, L.; Sun, L.; Becker, H.-C.; Åkermark, B.; Hammarström, L.; Ott, S. Bio-inspired, Side-on Attachment of a Ruthenium Photosensitizer to an Iron Hydrogenase Active Site Model. *Dalton Trans.* **2006**, 4599-4606.
28. Kluwer, A. M.; Kapre, R.; Hartl, F.; Lutz, M.; Spek, A. L.; Brouwer, A. M.; van Leeuwen, P. W. N. M.; Reek, J. N. H. Self-assembled Biomimetic [2Fe2S]-Hydrogenase-based Photocatalyst for Molecular Hydrogen Evolution. *Proc. Natl. Acad. Sci. U.S.A.* **2009,** *106*,10460-10465.
29. Li, B.; Liu, T.; Popescu, C. V.; Bilko, A.; Darensbourg, M. Y. Synthesis and Mössbauer Characterization of Octahedral Iron(II) Carbonyl Complexes $FeI_2(CO)_3L$ and $FeI_2(CO)_2L_2$: Developing Models of the [Fe]-H2ase Active Site. *Inorg. Chem.* **2009,** *48*, 11283-11289.

30. Magnuson, A.; Anderlund, M.; Johansson, O.; Lindblad, P.; Lomoth, R.; Polivka, T.; Ott, S.; Stensjo, K.; Styring, S. R.; Sundstrom, V.; Hammarstrom, L. Biomimetic and Microbial Approaches to Solar Fuel Generation. *Acc. Chem. Res.* **2009,** *42*, 1899-1909.
31. Ott, S.; Borgstrom, M.; Kritikos, M.; Lomoth, R.; Bergquist, J.; Åkermark, B.; Hammarstrom, L.; Sun, L. Model of the Iron Hydrogenase Active Site Covalently Linked to a Ruthenium Photosensitizer: Synthesis and Photophysical Properties. *Inorg. Chem.* **2004,** *43*, 4683-4692.
32. Ott, S.; Kritikos, M.; Åkermark, B.; Sun, L. Synthesis and Structure of a Biomimetic Model of the Iron Hydrogenase Active Site Covalently Linked to a Ruthenium Photosensitizer. *Angew. Chem. Int. Ed.* **2003,** *42*, 3285-3288.
33. Song, L. C.; Tang, M. Y.; Mei, S. Z.; Huang, J. H.; Hu, Q. M. The Active Site Model for Iron-Only Hydrogenases Coordinatively Bonded to a Metalloporphyrin Photosensitizer. *Organometallics* **2007,** *26*, 1575-1577.
34. Song, L.-C.; Liu, X.-F.; Ming, J.-B.; Ge, J.-H.; Xie, Z.-J.; Hu, Q.-M. Reactions Starting from Diiron Propanedithiolate [(Î¼-SCH2)2CH(OH)]Fe2(CO)6 Leading to Malonyl-, PPh3-, and [60]Fullerene-Containing Compounds Relevant to the Active Site of FeFe-Hydrogenases. *Organometallics* **2010,** *29*, 610-617.
35. Song, L.-C.; Wang, L.-X.; Tang, M.-Y.; Li, C.-G.; Song, H.-B.; Hu, Q.-M. Synthesis, Structure, and Photoinduced Catalysis of [FeFe]-Hydrogenase Active Site Models Covalently Linked to a Porphyrin or Metalloporphyrin Moiety *Organometallics* **2009,** *28*, 3834-3841.
36. Sun, L.; Åkermark, B.; Ott, S. Iron Hydrogenase Active Site Mimics in Supramolecular Systems Aiming for Light-driven Hydrogen Production. *Coord. Chem. Rev.* **2005,** *249* (15-16), 1653-1663.
37. Wolpher, H.; Borgstrom, M.; Hammarstrom, L.; Bergquist, J.; Sundstrom, V.; Styring, S.; Sun, L.; Akermark, B., Synthesis and Properties of an Iron Hydrogenase Active Site Model Linked to a Ruthenium Tris-bipyridine Photosensitizer. *Inorg. Chem. Commun.* **2003,** *6*, 989-991.
38. Bingaman, J. L.; Kohnhorst, C. L.; Van Meter, G. A.; McElroy, B. A.; Rakowski, E. A.; Caplins, B. W.; Gutowski, T. A.; Stromberg, C. J.; Webster, C. E.; Heilweil, E. J. Time-Resolved Vibrational Spectroscopy of [FeFe]-Hydrogenase Model Compounds. *J. Phys. Chem. A* **2012,** *116*, 7261-7271.
39. Bonner, G. M.; Ridley, A. R.; Ibrahim, S. K.; Pickett, C. J.; Hunt, N. T. Probing the Effect of the Solution Environment on the Vibrational Dynamics of an Enzyme Model System with Ultrafast 2D-IR Spectroscopy. *Faraday Discuss.* **2010,** *145*, 429-442.
40. Johnson, M.; Thuman, J.; Letterman, R. G.; Stromberg, C. J.; Webster, C. E.; Heilweil, E. J. Time-Resolved Infrared Studies of a Trimethylphosphine Model Derivative of [FeFe]-Hydrogenase. *J. Phys. Chem. B* **2013,** *117*, 15792-15803.
41. Kania, R.; Frederix, P. W. J. M.; Wright, J. A.; Ulijn, R. V.; Pickett, C. J.; Hunt, N. T. Solution-phase Photochemistry of a [FeFe]Hydrogenase Model Compound: Evidence of Photoinduced Isomerisation. *J. Chem. Phys.* **2012,** *136*, 044521-044529.
42. Kaziannis, S.; Santabarbara, S.; Wright, J. A.; Greetham, G. M.; Towrie, M.; Parker, A. W.; Pickett, C. J.; Hunt, N. T. Femtosecond to Microsecond Photochemistry of a [FeFe]hydrogenase Enzyme Model Compound. *J. Phys. Chem. B* **2010,** *114*, 15370-15379.
43. Ridley, A. R.; Stewart, A. I.; Adamczyk, K.; Ghosh, H. N.; Kerkeni, B. N.; Guo, Z. X.; Nibbering, E. T. J.; Pickett, C. J.; Hunt, N. T. Multiple-Timescale Photoreactivity of a Model

Compound Related to the Active Site of [FeFe]-Hydrogenase. Inorg. Chem. 2008**,** *47*, 7453-7455.
44. Stewart, A. I.; Clark, I. P.; Towrie, M.; Ibrahim, S. K.; Parker, A. W.; Pickett, C. J.; Hunt, N. T.Structure and Vibrational Dynamics of Model Compounds of the [FeFe]-Hydrogenase Enzyme System via Ultrafast Two-Dimensional Infrared Spectroscopy. *J. Phys. Chem. B* **2008,** *112*, 10023-10032.
45. Stewart, A. I.; Wright, J. A.; Greetham, G. M.; Kaziannis, S.; Santabarbara, S.; Towrie, M.; Parker, A. W.; Pickett, C. J.; Hunt, N. T. Determination of the Photolysis Products of [FeFe]Hydrogenase Enzyme Model Systems using Ultrafast Multidimensional Infrared Spectroscopy. *Inorg. Chem.* **2010,** *49*, 9563-9573.
46. Caplins, B. W.; Lomont, J. P.; Nguyen, S. C.; Harris, C. B. Vibrational Cooling Dynamics of a [FeFe]-Hydrogenase Mimic Probed by Time-Resolved Infrared Spectroscopy. *The Journal of Physical Chemistry A* **2014,** *118*, 11529-11540.
47. Razavet, M.; Davies, S. C.; Hughes, D. L.; Pickett, C. J. {2Fe3S} Clusters Related to the Di-iron Sub-site of the H-centre of all-Iron Hydrogenases. *Chem. Commun.* **2001,** 847-848.
48. Siegbahn, P. E. M.; Tye, J. W.; Hall, M. B. Computational Studies of [NiFe] and [FeFe] Hydrogenases. *Chem. Rev.* **2007,** *107*, 4414-4435.
49. Tard, C.; Pickett, C. J. Structural and Functional Analogues of the Active Sites of the [Fe]-, [NiFe]-, and [FeFe]-Hydrogenases *Chem. Rev.* **2009,** *109*, 2245-2274.
50. Zampella, G.; Bruschi, M.; Fantucci, P.; Razavet, M.; Pickett, C. J.; De Gioia, L. Dissecting the Intimate Mechanism of Cyanation of {2Fe3S} Cmplexes Related to the Active Site of All-Iron Hydrogenases by DFT Analysis of Energetics, Transition States, Intermediates and Products in the Carbonyl Substitution Pathway. *Chem. Eur. J.* **2005,** *11*, 509-520.
51. Lyon, E. J.; Georgakaki, I. P.; Reibenspies, J. H.; Darensbourg, M. Y. Carbon Monoxide and Cyanide Ligands in a Classical Organometallic Complex Model for Fe-Only Hydrogenase. *Angew. Chem. Int. Ed.* **1999,** *38*, 3178-3180.
52. Gilbert-Wilson, R.; Siebel, J. F.; Adamska-Venkatesh, A.; Pham, C. C.; Reijerse, E.; Wang, H.; Cramer, S. P.; Lubitz, W.; Rauchfuss, T. B. Spectroscopic Investigations of [FeFe] Hydrogenase Maturated with [57Fe2(adt)(CN)2(CO)4]2–. *Journal of the American Chemical Society* **2015,** *137*, 8998-9005.
53. Roy, L. E.; Batista, E. R.; Hay, P. J. Theoretical Studies on the Redox Potentials of Fe Dinuclear Complexes as Models for Hydrogenase. *Inorganic Chemistry* **2008,** *47*, 9228-9237.
54. Manor, B. C.; Ringenberg, M. R.; Rauchfuss, T. B. Borane-Protected Cyanides as Surrogates of H-Bonded Cyanides in [FeFe]-Hydrogenase Active Site Models. *Inorganic Chemistry* **2014,** *53*, 7241-7247.
55. Yu, L.; Greco, C.; Bruschi, M.; Ryde, U.; De Gioia, L.; Reiher, M. Targeting Intermediates of [FeFe]-Hydrogenase by CO and CN Vibrational Signatures. *Inorganic Chemistry* **2011,** *50* (9), 3888-3900.
56. Justice, A. K.; Linck, R. C.; Rauchfuss, T. B. Diruthenium Dithiolato Cyanides: Basic Reactivity Studies and a Post Hoc Examination of Nature's Choice of Fe versus Ru for Hydrogenogenesis. *Inorganic Chemistry* **2006,** *45*, 2406-2412.
57. Fiedler, A. T.; Brunold, T. C. Combined Spectroscopic/Computational Study of Binuclear Fe(I)−Fe(I) Complexes: Implications for the Fully-Reduced Active-Site Cluster of Fe-Only Hydrogenases. *Inorganic Chemistry* **2005,** *44* (6), 1794-1809.
58. Kaziannis, S.; Wright, J. A.; Candelaresi, M.; Kania, R.; Greetham, G. M.; Parker, A. W.; Pickett, C. J.; Hunt, N. T. The role of CN and CO ligands in the vibrational relaxation dynamics

of model compounds of the [FeFe]-hydrogenase enzyme. *Phys. Chem. Chem. Phys.* **2011,** *13*, 10295-10305.
59. Hunt, N. T.; Wright, J. A.; Pickett, C. Detection of Transient Intermediates Generated from Subsite Analogues of [FeFe] Hydrogenases. *Inorganic Chemistry* **2016,** *55*, 399-410.
60. Frederix, P. W. J. M.; Adamczyk, K.; Wright, J. A.; Tuttle, T.; Ulijn, R. V.; Pickett, C. J.; Hunt, N. T.Investigation of the Ultrafast Dynamics Occurring during Unsensitized Photocatalytic H2 Evolution by an [FeFe]-Hydrogenase Subsite Analogue. *Organometallics* **2014,** *33*, 5888-5896.
61. Certain commercial equipment or materials are identified in this paper to adequately specify the experimental procedures. In no case does the identification imply recommendation or endorsement by NIST, nor does it imply that the materials or equipment identified are necessarily the best available for the purpose.
62. Parr, R. G.; Yang, W., *Density-Functional Theory of Atoms and Molecules*. Oxford University Press: New York, 1989.
63. Frisch, M. J.; Trucks, G. W.; Schlegel, H. B.; Scuseria, G. E.; Robb, M. A.; Cheeseman, J. R.; Scalmani, G.; Barone, V.; Mennucci, B.; Petersson, G. A. et al.. *Gaussian 09 Revision A.02*, Gaussian Inc.: Wallingford, CT, 2009.
64. Becke, A. D. Density-Functional Exchange-Energy Approximation with Correct Asymptotic Behavior. *Phys. Rev. A* **1988,** *38*, 3098-3100.
65. Perdew, J. P. Density-functional Approximation for the Correlation Energy of the Inhomogeneous Electron Gas. *Phys. Rev. B* **1986,** *33*, 8822-8824.
66. Perdew, J. P. Erratum: Density-functional Approximation for the Correlation Energy of the Inhomogeneous Electron Gas. *Phys. Rev. B* **1986,** *34*, 7406-7406.
67. Schafer, A.; Horn, H.; Ahlrichs, R. Fully Optimized Contracted Gaussian Basis Sets for Atoms Li to Kr. *J. Chem. Phys.* **1992,** *97*, 2571-2577.
68. Schafer, A.; Huber, C.; Ahlrichs, R. Fully Optimized Contracted Gaussian Basis Sets of Triple Zeta Valence Quality for Atoms Li to Kr. *J. Chem. Phys.* **1994,** *100*, 5829-5835.
69. Meyer, R. L.; Zhandosova, A. D.; Biser, T. M.; Heilweil, E. J.; Stromberg, C. J. Photochemical dynamics of a trimethyl-phosphine derivatized [FeFe]-hydrogenase model compound. *Chemical Physics* **2018**, https://doi.org/10.1016/j.chemphys.2017.12.014

70. Silaghi-Dumitrescu, I.; Bitterwolf, T. E.; King, R. B. Butterfly Diradical Intermediates in Photochemical Reactions of Fe2(CO)6(μ-S2). *J. Am. Chem. Soc.* **2006,** *128*, 5342-5343.
71. Eckert, P. A.; Kubarych, K. J. Dynamic Flexibility of Hydrogenase Active Site Models Studied with 2D-IR Spectroscopy. J. Phys. Chem. A 2017**,** *121*, 608-615.

Table of Contents Graphic (TOC)